MICRODOPING OF LAYERS FOR HIGH EFFICIENCY SILICON HETEROJUNCTION SOLAR CELLS

I. Voicu Vulcanean[1], J. Seif[2], S. Pingel[1], I. Koc[1], M. Bivour[1], A. Steinmetz[1]
[1]Fraunhofer Institute for Solar Energy Systems ISE, Germany
[2]Idener, Spain

ABSTRACT: Within this paper two approaches have been attempted to improve the interfaces of silicon heterojunction devices, either intrinsic amorphous silicon a-Si:H(i) to doped layer a-Si:H(n) or a-Si:H(i) layer to silicon oxide and nanocrystalline layer nc-Si:H (n or p). For the conventional a-Si:H based device, microdoping was implemented in the i2 layer of the a-Si:H(i) layer stack, aiming to increase the fill factor. An improvement in fill factor of up to 0.5%$_{abs.}$ was shown by introducing microdoping into a fraction of the i2 layer, resulting in an improved efficiency reaching 23.4% compared to the undoped reference at 23.2%. For "next generation" SHJ devices based on nc-Si:H, microdoping was implemented in the interfacial silicon oxide layer. For nc-Si:H(n) the fill factor showed a gain of up to 0.3%$_{abs.}$ compared with the undoped group, with the best cell reaching 22.9% efficiency. When introducing microdoping in the silicon oxide layer for nc-Si:H(p), a similar trend is observed as an increase in *FF* of ~0.3%$_{abs.}$ compared with undoped group drives the efficiency for the best cell at 23%. The two microdoping approaches decreased the series resistance, positively affecting the fill factor.
Keywords: silicon heterojunction solar cell, a-Si, nanocrystalline, microdoping, fill factor

1 INTRODUCTION

The progress in achieving high efficiency solar cells with silicon heterojunction (SHJ) devices has been substantial in recent years, with record energy conversion efficiencies reaching 26.81% [1]. The technology is known to exhibit high open-circuit voltages (V_{oc}), enabled by the excellent passivation properties of the hydrogenated amorphous silicon layers (a-Si:H) [2]. The layers are deposited in stacks with intrinsic (i) followed by n-doped amorphous layer for the front, and intrinsic (i) followed by p-doped amorphous layer for the rear. As next step, sputtering of transparent conductive oxide (TCO) is introduced for antireflection and lateral charge transport [3][4]. The amorphous silicon layers tend to limit the cell performance due to fill factor (*FF*) limitation, induced by high series resistance (R_s) [5]. Therefore, to further improve the device, a key factor in achieving higher efficiencies is to improve the *FF*. Besides improving the a-Si:H layer stack, nanocrystalline silicon layers are a viable solution to improve both optical and transport properties in SHJ solar cells. These layers exhibit lower absorption at shorter wavelengths, enabling higher short-circuit current densities (J_{sc}) [6]. In addition to this, improved transport properties and more efficient doping compared with a-Si:H, results in improved contacts [6]. In order to get the benefits of the nc-Si:H layers, several requirements have to be met: a) obtaining a fast nucleation of the nc-Si:H layer on top of the intrinsic a-Si:H layer; b) no damage to the passivation layer during nc-Si:H deposition; c) high crystallinity of the nc-Si:H layer to benefit from higher doping efficiency and transparency [7]. It has been shown that silicon oxide layers (SiO_x) grown prior to the nc-Si:H material, play an important role in helping to accelerate the nucleation of the nc-Si:H layers [5], thus obtaining thinner layers and subsequently improving the J_{sc}.

2 EXPERIMENTAL

The samples in this study were based on n-type monocrystalline Czochralski (Cz) M2 silicon wafers with a thickness of 160 µm (after texturing) and base resistivity of 1 Ωcm. The as-cut wafers have been subjected to saw damage removal, texturing and ozone-based cleaning followed by HF dip to remove the native oxide prior the deposition of the a-Si:H layers. The a-Si:H and nc-Si:H layers have been deposited by PECVD at 13.56 MHz, using SiH_4, H_2, PH_3 (5% in H_2), TMB (2% in H_2) and additional CO_2 (for SiO_x) as process gasses. The PECVD processes for the a-Si:H layers were conducted at 200°C, while for the nc-Si:H layers a temperature of 140°C was used.
Adding dopant gases in the mix for the i2 layer deposition changes the deposition rate of the standard process. The deposition rate of the microdoped layers was determined depositing layers on flat float-zone (FZ) silicon samples and characterizing them by means of spectroscopic ellipsometry. The deposition time was then adjusted to reach the same thickness as for the undoped reference. The samples were finalized by sputtered TCO followed by industrial screen-printing metallization. The final parameters of the manufactured SHJ cells are analyzed by I-V measurements under standard testing conditions (GridTouch, full area measurement, black non-reflecting chuck). All cells are processed in a rear emitter configuration (p-doped layer at the rear).

2.1 Microdoping the i2 layer of the a-Si:H(i) layer stack

A first approach was implemented for the amorphous layers for SHJ by microdoping fractions of the total thickness of the i2 layer (Figure 1). The dopant concentration and the overall thickness of the i2 layer were kept constant, only the doped layer thickness of the initial undoped i2 layer was changed in ¼ steps from 0% (undoped ref.) to 100% (completely doped i2 layer). A trade-off between maintaining the passivation and the generated current on a high enough level versus the potential improvement in the series resistance and the fill factor can be expected, as the potential improvement in the carrier transport from adding extra doping in the i2 layer can come at the cost of degradation in passivation and optical losses by decreasing the transparency of the layer.

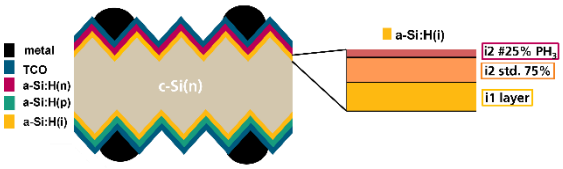

Figure 1: Schematic illustration of the SHJ solar cell structure with microdoping 25% of the thickness of the i2 layer.

2.2 Microdoping the interfacial SiO_x layer for nc-Si:H (n or p) devices

Following the second approach, the interfacial SiO_x seed-layers for subsequent nc-Si:H (either n or p) depositions were microdoped (Figure 2 & 3). The SiO_x layer can be grown via a vacuum break after a-Si:H deposition or by using a PECVD-based plasma treatment [8], as it was implemented for the experiments included in this paper. Before the implementation of the dopant in the SiO_x layer, variations in the SiO_x layer thickness have been conducted in order to optimize the process. The plasma treatment time has been varied for a CO_2 concentration of 5%. The thickness of the nc-Si:H doped layers was approximately 25 nm.

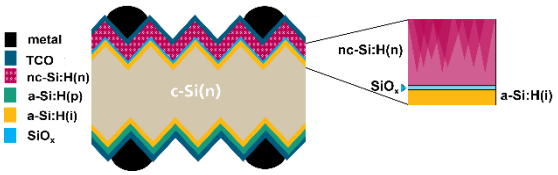

Figure 2: Schematic illustration of the SHJ solar cell structure with nc-Si:H(n).

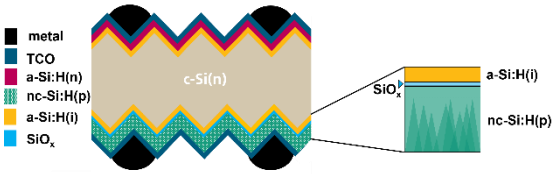

Figure 3: Schematic illustration of the SHJ solar cell structure with nc-Si:H(p).

3 RESULTS AND DISCUSSION

3.1 Microdoping the i2 for i/n layer stack

The results of implementing microdoping into the i2 layer are summarized in Figure 4. Clear trends can be seen in all cell parameters with increasing the fraction (#xx%) of the doped i2 layer. Strong impact on passivation is noticed with a decreasing V_{oc} with increasing the thickness fraction of the doped layer. While for the #25% group the loss in V_{oc} is below 1 mV, for the #100% group a V_{oc} drop of ~4 mV is observed compared to the undoped reference.

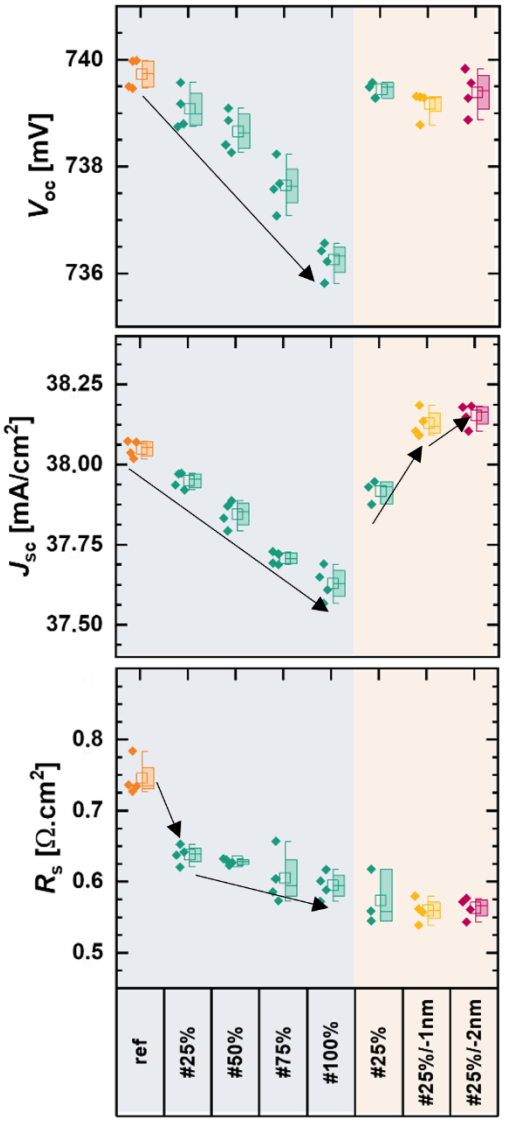

Figure 4:(A) I-V results obtained by microdoping fractions of the i2 layer thickness, increasing in ¼ steps from 0% (ref) to 100%.

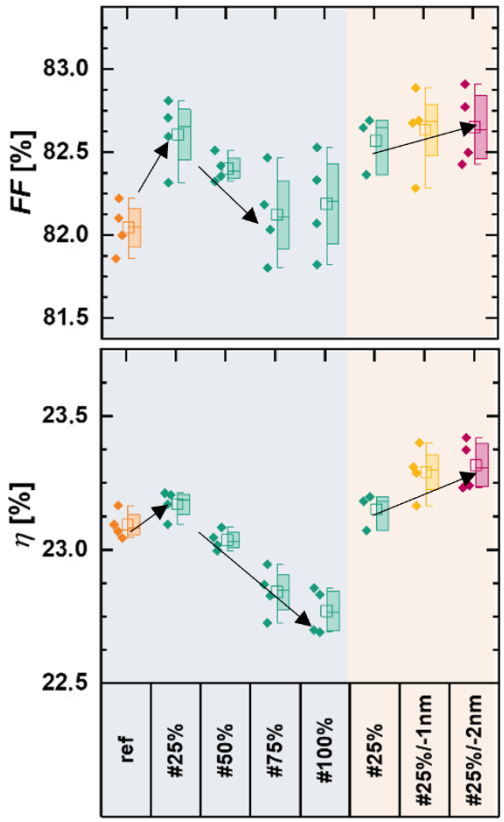

Figure 4:(B) I-V results for SHJ cells obtained by microdoping fractions of the i2 layer, increasing in ¼ steps from 0% (ref) to 100%.

Likely due to parasitic light absorption from the additional dopant included in the i2 layer, a downward trend is observed for the J_{sc}, recording losses of up to 0.5 mA/cm^2 from undoped to 100% doped layer. However, due to improved carrier transport at the interface and a drop in R_s, the *FF* increases above the undoped reference for all groups that have been subjected to microdoping. This values up to 0.5%$_{abs.}$ gain compared to the undoped reference, reaching a *FF* of 82.8% for the #25% group. This large boost in *FF* leads to roughly 0.1%$_{abs.}$ increase in efficiency. While doping larger fractions of the intrinsic layer shows lower R_s values, it is not enough to compensate for the degradation in passivation observed as decreasing V_{oc} and the optical losses indicated by lower J_{sc}.

To offset the losses due to microdoping of the i2 layer, the focus on the second experiment was to improve the J_{sc}. Therefore, the thickness of the standard n-doped layer was reduced. The process sequence for #25% group from the previous experiment is used as a reference. As both groups with thinner n-layer show an increase in J_{sc} of ~0.2 mA/cm^2 above the reference, we demonstrated that this approach has been successfully implemented. The V_{oc} didn't show major changes with all groups being in their standard deviation range. This is also the case for the *FF*. The J_{sc} improvement, together with a mean *FF* of ~82.6%, resulted in efficiencies of up to 23.4%.

3.2 Microdoping the SiO$_x$ seed-layers for nc-Si:H(n)

Implementing plasma treatment time variation for interfacial SiO$_x$ layers followed by the subsequent nc-Si:H(n) deposition leads to the results summarized in Figure 5.

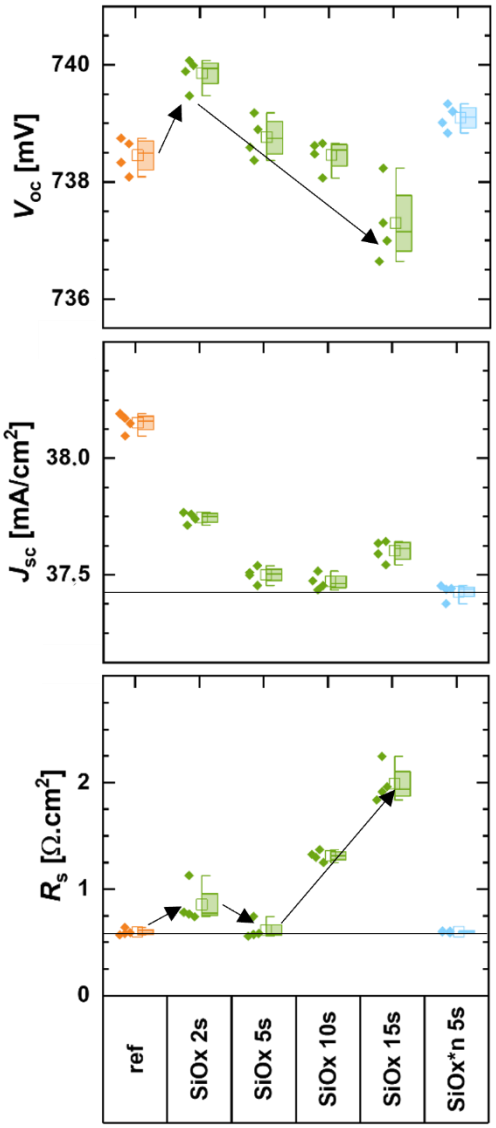

Figure 5:(A) I-V results for SHJ cells obtained with nc-Si:H(n) layers at the front, with variation in plasma treatment time, without and with microdoping for the SiO$_x$ layers present at the a-Si:H(i) interface.

An optimum between sufficiently thin SiO$_x$ layer for efficient charge carrier transport and sufficiently thick SiO$_x$ for adequate nucleation must be found. Ellipsometry results show a layer thickness between 0.4 nm at 2 s and 2 nm at 15 s. For the short plasma treatment time of 2 and 5 seconds the *FF* is on the same level as the reference. Beyond 5 seconds the charge carriers are not efficiently extracted anymore and a drop in *FF* and overall loss in conversion efficiency is observed, mainly due to an increase in R_s, up to 2 Ωcm^2. Based on mean reflection values (data not shown), the nc-Si:H(n) groups have shown lower reflection compared with the a-Si:H reference, however this is not enough to compensate the losses of ~20% in the short wavelength range. Additionally, a thicker nc-Si:H(n) layer by a factor of 3 compared to the a-Si:H(n) reference leads to a lower J_{sc}. The group with 5 s is chosen for microdoping due to better *FF* and a higher mean efficiency. Doping the SiO$_x$ layer

by small amounts with PH_3 (indicated as SiO_x*n) maintains low R_s and improves the *FF* up to 82.8%.

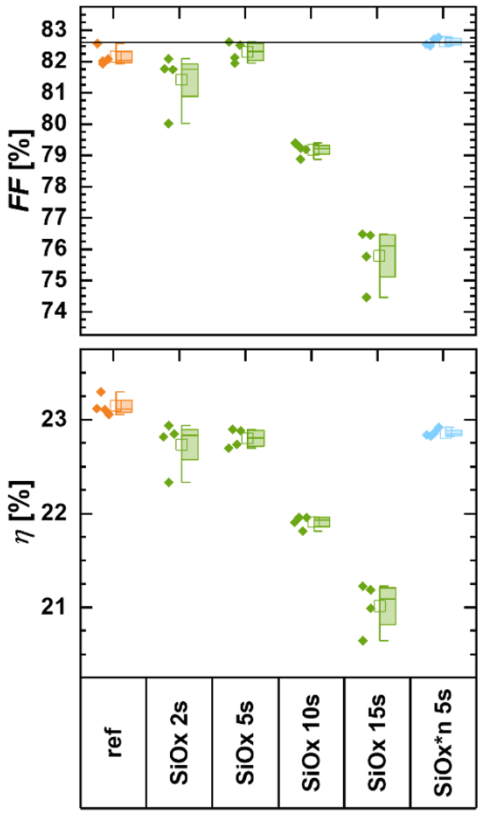

Figure 5:(B) I-V results obtained with nc-Si:H(n) layers at the front, with variation in deposition time for the SiOx layers present at the a-Si:H(i) interface.

Similar as for microdoping the i2 of the a-Si:H(i) layer stack due to transparency issues in the oxide layer as dopant is added, the SiO_x*n 5 s group shows lower J_{sc} values as the SiOx 5 s group, dropping below 37.5 mA/cm^2. Due to poor *FF*, the groups with long oxidation time fall in the range of 21 to 22% in efficiency. The efficiency for the nc-Si:H(n) group with short plasma treatment is close to 23%, while the SiO_x*n group being only slightly better due to improved *FF*.

3.3 Microdoping the SiO_x seed-layers for nc-Si:H(p)

Implementing nc-Si:H(p) on the rear side of the SHJ cells (see Figure 3) leads to the results summarized in Figure 6. To evaluate the benefits of nc-Si:H(p) layers for bi-facial applications, the cells were measured from the front (FS - green symbols) and rear (RS - orange symbols) side. Based on the results from the nc-Si:H(n) experiment, the SiO_x with a plasma treatment time of 5 seconds was chosen as a starting point, followed by a group with added dopant in the oxide layer (indicated as SiO_x*p) and the last group (indicated as SiO_x**p) for which we increased the doping concentration. The difference in J_{sc} between the FS and RS by more than 2 mA/cm^2 for all groups is caused by a lower reflection on the front side. The slightly better J_{sc} for the nc-Si:H(p) films from the rear side measurement can be attributed to a better IR response. Controversial trends can be seen for the J_{sc} where the heavy doped group (SiOx**p) gains ~0.1 mA/cm² for the FS. However, for the RS measurement a downward trend in J_{sc} can be seen as we increase the doping concentration. The SiO_x*p group achieves a similar V_{oc} (739-740 mV- data not shown), in comparison to the undoped group and the a-Si:H reference. A downward trend can be observed for the R_s (rear side measurement), as the series resistance drops from the undoped SiO_x group to the doped SiO_x (p* and p**) groups by ~0.1 Ωcm^2. As for microdoping of the SiO_x*n, an improvement of ~0.3%$_{abs.}$ in *FF* is reached for the SiO_x p** group (RS). These gains bring the SiO_x**p group to a mean efficiency of 22.7%, with the champion cell reaching a conversion efficiency of 23%.

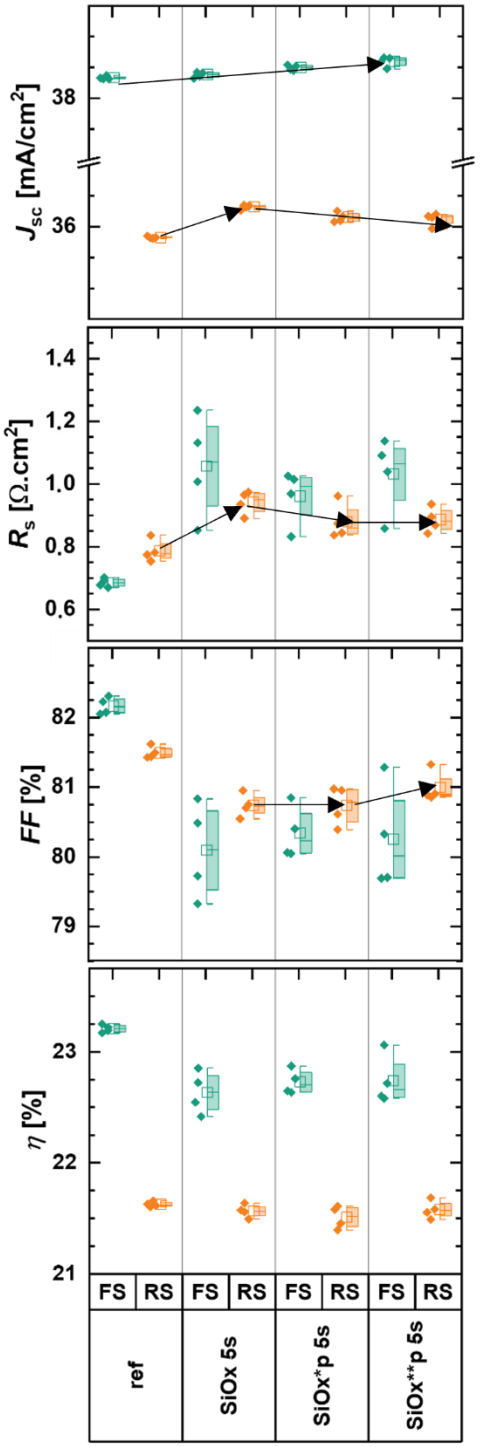

Figure 6: I-V results obtained with nc-Si:H(p) layers at the rear, with microdoping variation for the SiO_x layers present at the a-Si:H(i) interface. Front side (FS) and rear side (RS) measurements are shown.

4 CONCLUSION

In this paper we showed a promising way to improve the interface of the SHJ layers, and subsequently the *FF* via microdoping. For a classic a-Si:H based SHJ device, doping a fraction of the total thickness of the i2 layer showed a drop in J_{sc} and Voc but these losses were compensated by improved carrier transport via decreasing the R_s, which resulted in a *FF* gain of up to $0.5\%_{abs.}$ for the #25% group. improving the efficiency up to 23.4% compared to the undoped reference 23.2%. A similar approach has been used for "next generation" SHJ devices based on nc-Si:H by doping the interfacial SiO_x for nc-Si:H (n or p). We observed an improvement by lowering the R_s, resulting in a positive trend for the *FF*, for both front and rear layers.
For nc-Si:H(n) with the SiOx*n group, the *FF* showed a gain of up to $0.3\%_{abs.}$ compared with the undoped group, with the best cell reaching 22.9% efficiency. Introducing microdoping in the SiO_x for nc-Si:H(p), a similar trend is observed as an increase in *FF* of ~$0.3\%_{abs.}$ compared with undoped group drives the efficiency for the best cell at 23%. Reducing the J_{sc} gap of nc-Si:H based solar cell device compared to the a-Si:H will be a focus point for further optimization and will be addressed by reducing the thickness of the doped nc-Si:H layers.

FUNDING

This work was supported by the German Federal Ministry for Economic Affairs and Climate Action BMWK within the research project "Utility4Indium" under contract no. 03EE1127D.

ACKNOWLEDGEMENT

The authors would like to thank all colleagues from the PV division contributing to this work for sample preparation and characterization.

REFERENCES

[1] LONGi Green Energy Technology Co., Ltd. (LONGi). At 26.81%, LONGi sets a new world record efficiency for silicon solar cells. Xi'an, China; 19.11.2022.

[2] Duan W, Lambertz A, Bittkau K, Qiu D, Qiu K, Rau U, Ding K. A route towards high-efficiency silicon heterojunction solar cells. Progress in Photovoltaics. 2022;30:384–92. doi:10.1002/pip.3493.

[3] Mazzarella L, Morales-Vilches AB, Korte L, Schlatmann R, Stannowski B. Ultra-thin nanocrystalline n-type silicon oxide front contact layers for rear-emitter silicon heterojunction solar cells. Solar Energy Materials and Solar Cells. 2018;179:386–91. doi:10.1016/j.solmat.2018.01.034.

[4] Antognini, Luca; Paratte, Vincent; Haschke, Jan; Cattin, et al. Influence of the Dopant Gas Precursor in P-Type Nanocrystalline Silicon Layers on the Performance of Front Junction Heterojunction Solar Cells. IEEE J. Photovoltaics. 10.1109/JPHOTOV.2021.3074072

[5] Boccard M, Monnard R, Antognini L, Ballif C. Silicon oxide treatment to promote crystallinity of p-type microcrystalline layers for silicon heterojunction solar cells. In: SiliconPV2018. p. 40003. doi:10.1063/1.5049266.

[6] Nogay G, Seif JP, Riesen Y, Tomasi A, Jeangros Q, Wyrsch N, et al. Nanocrystalline Silicon Carrier Collectors for Silicon Heterojunction Solar Cells and Impact on Low-Temperature Device Characteristics. IEEE J. Photovoltaics. 2016;6:1654–62. doi:10.1109/JPHOTOV.2016.2604574.

[7] Seif JP, Descoeudres A, Nogay G, Hanni S, Nicolas SM de, Holm N, et al. Strategies for Doped Nanocrystalline Silicon Integration in Silicon Heterojunction Solar Cells. IEEE J. Photovoltaics. 2016;6:1132–40. doi:10.1109/JPHOTOV.2016.2571619.

[8] Steinmetz A, Seif J, Koc I, Voicu Vulcanean I, Kurt D, Pingel S, Bivour M. Nanocrystalline Silicon Layer for the Application in Silicon Heterojunction Solar Cells. SiliconPV 2023 Conference. To be published.